Growth morphologies of crystal surfaces

Rong-Fu Xiao, J. Iwan D. Alexander, and Franz Rosenberger
Center for Microgravity and Materials Research, University of Alabama in Huntsville, Huntsville, Alabama 35899
(Received 31 August 1990)

We have expanded our earlier Monte Carlo model [Phys. Rev. A **38**, 2447 (1988); J. Crystal Growth **100**, 313 (1990)] to three dimensions and included reevaporation after accommodation and growth on dislocation-induced steps. We found again that, for a given set of growth parameters, the critical size, beyond which a crystal cannot retain its macroscopically faceted shape, scales linearly with the mean free path in the vapor. However, the three-dimensional (3D) the systems show increased shape stability compared to corresponding 2D cases. Extrapolation of the model results to mean-free-path conditions used in morphological stability experiments leads to order-of-magnitude agreement of the predicted critical size with experimental findings. The stability region for macroscopically smooth (faceted) surfaces in the parameter space of temperature and supersaturation depends on both the surface and bulk diffusion. While surface diffusion is seen to smooth the growth morphology on the scale of the surface diffusion length, bulk diffusion is always destabilizing. The atomic surface roughness increases with increase in growth temperature and supersaturation. That is, the tendency of surface kinetics anisotropies to stabilize the growth shape is reduced through thermal and kinetic roughening. It is also found that the solid-on-solid assumption, which can be advantageously used at low temperatures and supersaturations, is insufficient to describe the growth dynamics of atomically rough interfaces where bulk diffusion governs the process. For surfaces with an emerging screw dislocation, we find that the spiral growth mechanism dominates at low temperatures and supersaturations. The polygonization of a growth spiral decreases with increasing temperature or supersaturation. When the mean free path in the nutrient is comparable to the lattice constant, the combined effect of bulk and surface diffusion reduces the terrace width of a growth spiral in its center region. At elevated temperatures and supersaturations, 2D nucleation-controlled growth can dominate in corner and edge regions of a facet, while the spiral growth mode prevails in its center. Thus, in addition to confirming the experimental observation that the critical size of a growing crystal depends on the prevailing growth mechanism, we are able to obtain detailed insight into the processes leading to the loss of face and facet stability.

I. INTRODUCTION

Since the first application of the Monte Carlo (MC) method to simulations of crystal growth by Chernov and Lewis[1,2] its use has become widespread. MC studies were concerned with equilibrium and growth morphologies of crystals,[3–5] surface-roughening transitions[6–9] and growth-rate dependence on supersaturation and temperature.[10,11] For reviews see Refs. 12 and 13. These studies were primarily focused on interfacial kinetics and have occasionally included surface diffusion.[11] A solid-on-solid (SOS) restriction (no overhangs)[14] was often invoked. The influence of bulk diffusion, i.e., the transport of growth units through the nutrient to the interface, has received less attention until very recently.[15–18] In the event that surface diffusion and interfacial kinetics govern the growth morphology, these simplifications are not severe limitations. However, in reality, bulk transport often plays a decisive role in limiting morphological stability.[19–26]

Recently, we have studied the morphological evolution of growing crystals in two dimensions by considering both bulk transport and anisotropic interface kinetics.[15,16] For the bulk transport, we employed the diffusion-limited-aggregation model of Witten and Sander.[27] In the formulation of the interface kinetics we followed largely Gilmer and Bennema's work.[5,11] Through a systematic variation of the simulation parameters (temperature, bond strength, and supersaturation), the whole range of growth morphologies from fully faceted to side-branched dendritic growth was recovered. Our results show that the diffusion in the bulk nutrient and the anisotropy in the interface kinetics act morphologically destabilizing and stabilizing, respectively. For a given set of simulation parameters and symmetry of the lattice, there is a critical size beyond which a crystal cannot retain its stable, macroscopically faceted growth shape. This critical size scales linearly with the mean free path in the vapor.

In our previous studies[15,16] we ignored the fact that after attachment, the particles still have a finite probability to leave the attachment site. This approximation is valid when the system is far from equilibrium; i.e., the flux of particles impinging on the crystal surface largely exceeds that of the evaporating particles. However, close to equilibrium, the rates of impingement and evaporation are comparable. Then a more realistic description of crystal growth must account for the non-negligible chance that interfacial particles either move (diffuse) on the surface or evaporate back into the nutrient *at any*

time after the initial accommodation on the surface.

The growth of perfect crystals proceeds typically through two-dimensional-nucleation,[28] which is extremely slow at low temperatures and supersaturations. Yet, in reality, most crystals possess considerable concentrations of defects. Certain defects facilitate growth at low temperatures and supersaturations. Frank[29] found that a screw dislocation can provide an inexhaustible source of growth steps. Growth on dislocation-induced steps has since been observed experimentally by many workers,[30–24] and various theories for this growth mechanism have been proposed.[28,35–38] However, due to the complexity of the problem, no exact solutions have been obtained. Typical simplifications include the uniform spacing of growth steps and the neglect of nutrient bulk diffusion and surface diffusion. Although there have been some Monte Carlo simulations of dislocation-facilitated growth,[39,40] owing to the computational limitations at that time, the transport aspects of the problem were not taken into account.

In this paper we expand our previous studies[15,16] to three dimensions and investigate the role of two-dimensional (2D) nucleation growth and dislocation-induced growth in the morphological evolution of growing crystals. Instead of the multiple-registration scheme used in the earlier work to reduce microscopic noise,[15,16] we employ realistic reevaporation conditions for interfacial particles. The model and simulation procedure are described in Sec. II. Results on the influence of temperature and supersaturation on the surface morphology of perfect crystals are presented in Sec. III A. Based on a criterion originally proposed by Burton-Cabrera and Frank,[28] the thermal and kinetic roughening transitions are quantified. In addition, the scaling between the critical stable size of a faceted crystal and the mean free path of the vapor is studied in three dimensions. In Sec. III B we devote our effort to surfaces with dislocations and pay special attention to the shape and spacing of steps of growth spirals. We conclude the paper with results on the competition between normal growth at the corners and dislocation-facilitated growth at the center of a facet.

II. MODEL AND SIMULATION PROCEDURE

A. The model

Two different geometries, planar and spherical, are used to study the effect of bulk transport-induced nonuniformity in nutrient distribution on growth morphology. In the planar cases [Fig. 1(a)], the nutrient is contained between parallel crystal and source planes, which are infinite in lateral extent. In order to save computational time, we only consider a portion of the whole system and apply periodic boundary conditions in the x and y directions. In the other cases [Fig. 1(b)] a cubic seed is located at the center of a spherical source. Ideally, the separation between the growing crystal and the source should be infinite. But, again, to save computational time we choose a finite separation, yet one wide enough that the growth shape remains unbiased.[15] As a crystal grows, the distance between crystal surface and source is kept constant.

At molecular length scales, an individual growth unit undergoes generally several basic processes before becoming part of the growing crystal. After detachment from the source, a growth unit is transported by bulk diffusion towards the growing interface. The actual transport kinetics is determined by the interaction of growth units (or their precursors) and other species that form the nutrient. Usually, when a growth unit reaches the interface, it is not immediately incorporated into the growing crystal. It will adsorb and diffuse on the interface in an attempt to find an energetically favorable "final" attachment site, or

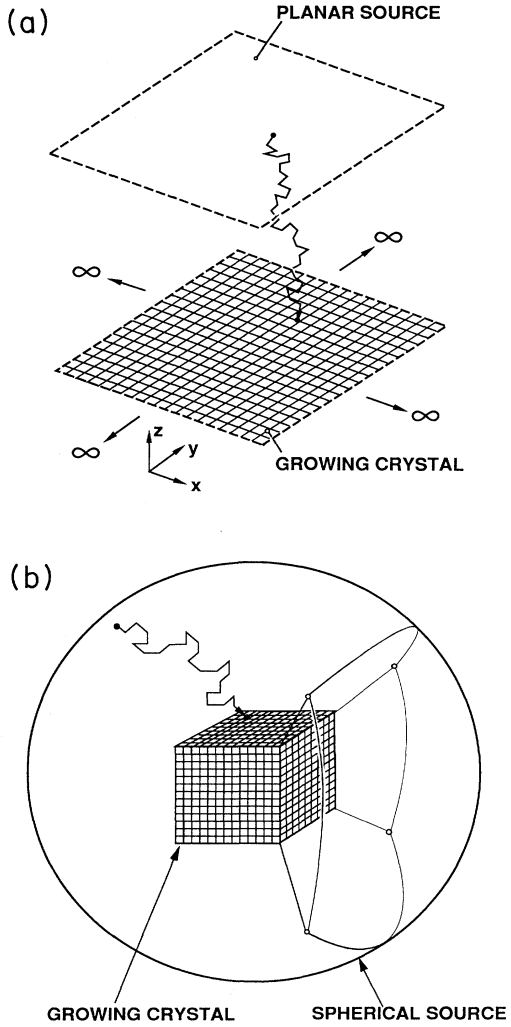

FIG. 1. Schematics of simulation geometries. (a) Planar case: lateral dimensions 60×60 lattice constants, with periodic boundary condition in the x and y directions. Space between crystal surface and source contains nutrient through which growth units diffuse to the crystal surface. (b) Spherical case: growing crystal in center of spherical source. Pyramidal section is used with periodic boundary conditions in azimuthal direction for simulation of 3D growth morphology at low temperatures; see text.

it will even return to the nutrient before it finds such a site. The latter happens, for instance, when the growth unit is misoriented and cannot form stable bonds with the crystal. Alternatively, the growth unit may impinge onto a site with too few neighbors to prevent it from being dislodged by thermal vibrations before it becomes adsorbed. A growth unit may even become dislodged after having arrived at an energetically favorable site. The probability that any of these processes occur is determined by the local configuration (arrangement of bond-forming neighbors) of the interface sites that the unit happens to visit. Though a complete model of such complex scenarios is not practical at this point, we have formulated a Monte Carlo model which retains the essential physics of both nutrient bulk transport and interface kinetics, including surface diffusion and reevaporation, without resorting to the SOS approximation.

We assume that the gaseous nutrient phase consists of two components: a growth species A, highly diluted in an inert gas B, such that the B concentration is essentially uniform and A-A interactions can be ignored. Component B randomizes the motion of A. Convection is ignored. The chemical potential is taken to be a linear function of the growth species concentration only. This results in a Fickian transport equation and, thus, a random walk may be used to describe diffusion in the nutrient phase in the form[15,16]

$$U(\mathbf{r},s\tau)=\frac{1}{c}\sum_{i}^{c}U(\mathbf{r}+\mathbf{a},(s-1)\tau) , \tag{1}$$

where $U(\mathbf{r},s\tau)$ is the probability that a walker can be found at location $\mathbf{r}$ after s steps (with a time interval τ) of jump length (mean free path) $|a|$. The normalization parameter c represents the total number of the possible jump sites.

To approximate the complex processes following the arrival of a growth unit on the interface, we make the following assumptions: The impingment rate K^+ can be obtained, based on ideal gas kinetics, from the chemical-potential difference $\Delta\mu$ between interfacial vapor and average surface site in the form[15]

$$K^+=K_{\rm eq}\exp(\Delta\mu/kT) , \tag{2}$$

where $K_{\rm eq}$ is the temperature-dependent equilibrium value of K^+. Note that in reality the overall driving force for the diffusion of A towards the crystal and subsequent interfacial attachment is the difference in chemical potential between the crystal surface and the source. Since we have accounted for bulk diffusion via a random-walk process, the chemical potential of the source does not appear explicitly in our model. The $\Delta\mu$ in Eq. (2) is therefore governed by the difference between the bulk-dependent vapor concentration at the interface and the equilibrium concentration at the same temperature. It should not be confused with the chemical-potential difference (bulk supersaturation, undercooling, etc.) used to control experimental crystal growth. This important point is discussed in more detail in Refs. 15 and 16 and also below.

The rates of both the evaporation and surface diffusion processes are sensitive to the local configuration of the site from which a unit is to be dislodged. Hence, following Gilmer and Bennema,[11] we write the evaporation rate K_i^- in the site-dependent form

$$K_i^-=\nu\exp(-E_i/kT) , \tag{3}$$

where ν is a lattice vibration factor and, in a nearest-neighbor approximation, E_i is simply the product of the pair-interaction (bond) energy ϕ of a unit with a nearest neighbor, and n_i is the number of occupied neighbor sites of site i.

For surface diffusion we assume that the diffusion rate depends on the occupation condition of both the site i that the particle occupies and the potential jump site j. Hence, we express the jump rate as

$$K_{i\to j}=\nu_s\exp(-\Delta E_{ij}/kT) , \tag{4}$$

where ν_s is a surface vibration factor, and the activation energy

$$\Delta E_{ij}=\begin{cases}\delta_i+\phi(n_i-n_j) & \text{for } n_i>n_j\\ \delta_i & \text{for } n_i\le n_j.\end{cases} \tag{5}$$

In reality, the term δ_i depends on the specific configuration i-j. For simplicity we have assumed that for a given i-j the δ term is independent of jump direction, hence the notation δ_i. As a consequence of this assumed direction independence, the δ_i terms cancel in the following formulations of transition probabilities and thus do not have to be calculated.

In real situations, impingment, surface diffusion, and evaporation take place at the same time with different magnitude. But in the MC simulation we consider one event at a time. Therefore, it is necessary to determine the sequence in which the events are to be considered. To this end we define an overall evaporation probability as

$$P^-=\frac{\overline{K^-}}{K^++\overline{K^-}} , \tag{6}$$

where $\overline{K^-}$ is the average "evaporation rate"

$$\overline{K^-}=\frac{1}{m}\sum_{i=1}^{m}K_i^- , \tag{7}$$

and the summation is over all m interfacial particles. By considering a local equilibrium condition for the kink site on a simple-cubic lattice, Eq. (6) becomes

$$P^-=\frac{B}{B+\exp(\Delta\mu/kT)\exp(-3\phi/kT)} , \tag{8}$$

with

$$B=\frac{1}{m}\sum_{i=1}^{m}\exp(-i\phi/kT) .$$

At equilibrium ($\Delta\mu/kT=0$), Eq. (8) yields $P^-\approx 0.5$; i.e., there are approximately equal amounts of particles evaporating from and impinging onto the crystal surface. At positive supersaturations ($\Delta\mu/kT>0$), P^- is less than 0.5; i.e., impingment exceeds evaporation. Correspond-

ingly, for negative supersaturations ($\Delta\mu/kT<0$), the P^- will be larger than 0.5, and more interfacial particles will evaporate and the crystal will shrink. These effects will not only be manifested in the growth and shrinkage rates, respectively, but will also influence the surface morphology.

After having decided the sequence of events, the individual probability for the various events needs to be determined. This depends on the specific site considered. For impingement, the probability, according to Eqs. (2) and (3), is $P_i^s=K^+/(K^++K_i^-)$. For a simple cubic crystal, this can be written as (for a derivation in 2D see Ref. 15)

$$P_i^s=\frac{\exp(\Delta\mu/kT)\exp[-(3-n_i)\phi/kT]}{1+\exp(\Delta\mu/kT)\exp[-(3-n_i)\phi/kT]} . \quad (9)$$

The jump probability from site i to a neighboring unoccupied site j (on the surface or in the nutrient), following Ref. 15 is

$$P_{i\to j}=\frac{K_{i\to j}}{\sum_{j=1}^{c'} K_{i\to j}}=\frac{\exp[-(n_i-n_j)\phi/kT)]}{\sum_{j=1}^{c'}\exp[-(n_i-n_j)\phi/kT)]} , \quad (10)$$

where c' is the number of unoccupied nearest-neighbor sites of site i. Clearly, a larger n_j results in a higher probability that a molecule will jump to site j on the interface.

The probability of evaporation for interfacial particles can be expressed as

$$P_i^e=\frac{K_i^-}{\sum_{i=1}^{m} K_i^-}=\frac{\exp(-n_i\phi/kT)}{mB}, \quad i=1,2,\ldots,m . \quad (11)$$

It can be seen from Eq. (11) that the probability of evaporation decreases exponentially with increasing number of solid bonds, and thus is highly anisotropic. The most probable sites for evaporation are those with the least solid neighbors, such as admolecules with a single solid bond. As the temperature and thus the surface roughness is increased, the anisotropy of the evaporation is decreased.

B. Simulation procedure

A summary of the simulation steps is presented in Fig. 2. First the initial conditions are chosen: for growth onto perfect crystals a smooth surface is set at a certain distance (typically 50 lattice units b, for $|a|=b$) from the source. In the planar case the surface is chosen as a square lattice measuring $60b\times 60b$, with periodic boundary conditions in x and y (lateral) directions. For growth onto dislocated crystals the lateral size is doubled in order to provide space for the evolution of several turns of a spiral. An initial dislocation is introduced by a vertical slip of parts of the lattice.[40] Note also that, as the crystal grows, the source is moved outwards such that the separation remains unchanged, as discussed in Ref. 15.

Following the setting of initial conditions and choice of specific input parameter values, P^- is calculated from ϕ, T, $\Delta\mu$ and the current crystal morphology. Comparison of a random number R with P^- determines the event to

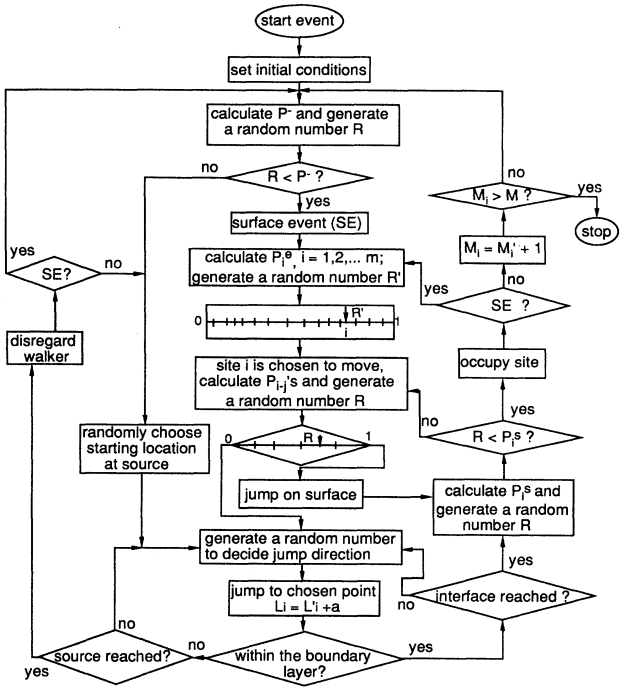

FIG. 2. Flow chart of simulation steps.

be considered. If $R>P^-$, a growth unit is released from the source and bulk diffusion is simulated through an isotropic sequence of random jumps of equal length (mean free path) $|a|$. Only when the particle has come within a distance $|a|$ from the crystal surface is a check implemented that determines whether the interface has been reached. The following steps, including the determination of average surface-diffusion lengths, are similar to our previous simulations except that we do not impose the multiple registration used in Refs. 15 and 16. A growth unit is tracked until it has either escaped from the system or is stuck onto the crystal surface.

If $R<P^-$, an evaporation event is selected. Then, all P_i^e $(i=1,\ldots m)$ are calculated from the recorded positions and neighboring configurations. Another random number R' is generated. If by chance R' falls into the ith interval, the ith interfacial particle is chosen to move. Then, governed by Eqs. (9), (10), and (11), the particle is kept moving until it has attached to some interfacial site or escaped to the source. If it sticks on site j, the local P_j^e's around the new site j as well as the earlier site i where the particle originated are recalculated. By using a new random number, a new evaporation event is selected. The evaporation route is pursued until some particle has escaped to the source. When this happens the P^- is recalculated and a new event is selected.

The simulation is continued until a desired size or layer thickness is reached. In a planar case, the simulation is continued until 14 400 or 10 000 particles, respectively,

have been added to a perfect or dislocated surface. In a spherical case, the simulation is stopped after a crystal has become unstable (the criterion for the instability will be discussed later). Typical CPU times were around 3 000–10 000 s on a Cray X-MP/24 and 5–50 h on an Ardent computer.

Our model has been designed for computational efficiency. As outlined above [see Eqs. (6)–(8)], the event to be considered is decided upon before the execution based on physical criteria rather than random choice only. In this way, any "unnecessary" operation is avoided. For example, evaporation will be executed whenever a random number R is less than P^-, although the selection of the actual execution site is quite random. In the earlier models,[11,40] the selection of a particle and calculation of the evaporation probability do not necessarily lead to an actual execution of an evaporation process. Many interfacial particles may have to be selected before a real evaporation event takes place. This is particularly time consuming under conditions of low temperature and supersaturation, in which the interface is rather smooth and the probability of evaporation is very low.

Note that, unless stated otherwise, the simulations were carried out with the magnitude of the mean free path in the vapor equal to one lattice constant $|a|=b$.

III. RESULTS AND DISCUSSION

A. Perfect surfaces

1. *Effects of surface and bulk diffusion at various temperatures*

As references for the more complex cases to be treated later and for comparison with earlier work,[6–9] we have first examined cases in which both bulk and surface diffusion were neglected. Particles arriving at random locations of the crystal either stick or are discarded. Figure 3 shows the effect of growth temperature or bond strength (i.e., ϕ/kT) on the morphology of a planar crystal surfaces at a constant low value of $\Delta\mu/kT=0.35$. At low temperature, as can be seen from Fig. 3(a), the growing crystal is atomically smooth with occasional 2D clusters on the surface; i.e., growth occurs by 2D nucleation only.[28] As the temperature increases [Fig. 3(b)] the surface becomes rougher and more 2D clusters with smaller size are formed on the surface and even on top of large clusters. On further increase in temperature the whole surface becomes atomically rough [Fig. 3(d)], and large size clusters can hardly be discerned. In this situation the crystal grows more readily due to the disappearance of the energy barrier for 2D nucleation. This thermal roughening effect has been extensively studied before under equilibrium conditions.[6–9,12,13] The earlier studies basically employed an algorithm for random pair exchange controlled by a Boltzmann factor $\exp(-\Delta E/kT)$. At equilibrium, the validity of the algorithm is guaranteed by the thermodynamic principle of path independence. For a nonequilibrium situation the random pair exchange algorithm is no longer valid. The final result depends not only on the potential energy between the initial and final sites but also on the actual path of the particles. In contrast, our model, as discussed in Sec. II, is more general and can be used in both equilibrium and nonequilibrium situations.

To further demonstrate the effect of temperature on the morphology of a growing crystal, we have plotted in Fig. 4 the surface area normalized by the area of a perfectly smooth surface versus the number of attached particles (in units of completed layers). The four curves correspond to cases (a)–(d) in Fig. 3. As can be seen from Fig. 4, at the lowest temperature the surface area oscillates periodically with minima on layer completion, alternating with maxima at about half-filled layers. Thus

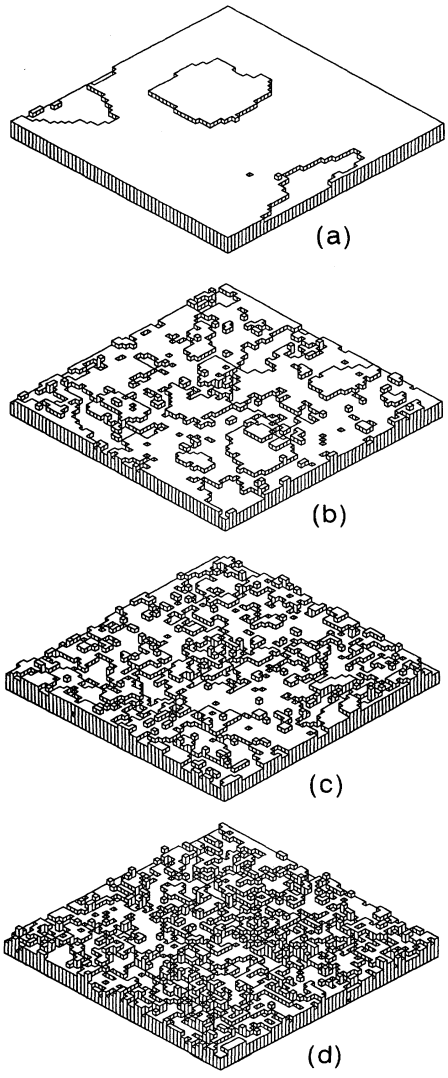

FIG. 3. Effect of temperature and bond strength on crystal surface morphologies at fixed supersaturation, $\Delta\mu/kT=0.35$. Both surface and bulk diffusion are excluded. (a) $\phi/kT=3.9$, (b) $\phi/kT=2.0$, (c) $\phi/kT=1.6$, (d) $\phi/kT=1.4$.

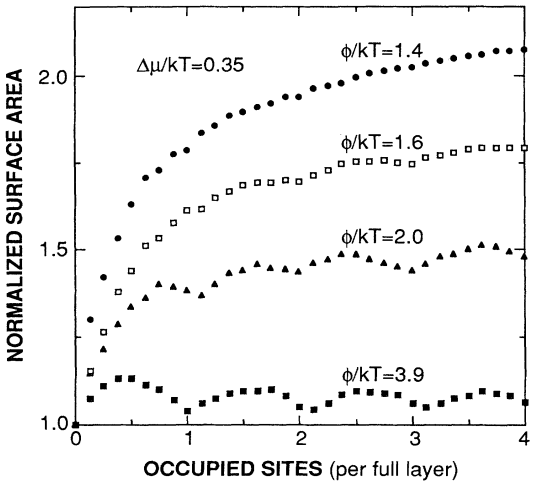

FIG. 4. Normalized surface area as function of number of attached particles (in units of full layer, i.e., 3600 particles). The normalization is based on the area of a perfectly smooth surface. The growth conditions are the same as in Fig. 3.

growth proceeds essentially layer by layer. When, following the formation of a 2D nucleus, a layer spreads, the surface area increases until a half-filled-layer state is reached and then decreases until that layer is completed. However, when the temperature is increased and thus the surface becomes rougher, the distinction between a half-filled layer and completed layers is blurred; i.e., new layers form before completion of the earlier layers. With increasing roughness, the periodicity disappears and the surface becomes delocalized.

Figure 5 illustrates the consequences of surface diffusion. Bulk diffusion is not considered in these examples with $\phi/kT=1.6$, $\Delta\mu/kT=0.69$. It can be seen that with surface diffusion [Fig. 5(b)] the crystal surface is much smoother than without surface diffusion [Fig. 5(a)]. The reason is that surface diffusion can provide an additional way for interfacial particles to relax to some energetically more favorable (low-energy) sites, and hence reduces the amplitude of the surface roughness. Of course, as we have shown before,[16] such a stabilizing contribution is effective only at a length scale comparable to the surface diffusion length, which, in turn, is sensitive to the surface roughness.[16] Generally speaking, the smoother a surface is, the farther an interfacial particle can diffuse during its lifetime on the surface. Hence, as shown by the simulation results of Fig. 6, the surface diffusion length decreases with increasing temperature. In addition to the temperature effect, Fig. 6 also reveals a strong dependence of surface diffusion length on supersaturation. This was not taken into account in earlier simulations,[11] in which the surface diffusion length was considered as an externally adjustable parameter, independent of temperature and supersaturation. By contrast, in our model, surface diffusion is an integral part of the attachment and evaporation processes.

Unlike surface diffusion, bulk diffusion acts destabilizing on the interface morphology.[15–17] This is shown in Fig. 7 for a case with surface diffusion, $\Delta\mu/kT=3.0$ and $\phi/kT=2.3$. For the three subfigures, the mean free path in the nutrient was decreased from "infinite" [Fig. 7(a)] to ten [Fig. 7(b)] and one crystal lattice constant [Fig. 7(c)], respectively. The infinite mean free path corresponds to direct jumps of growth units from the source onto the crystal surface, as in the simulations leading to Figs. 3

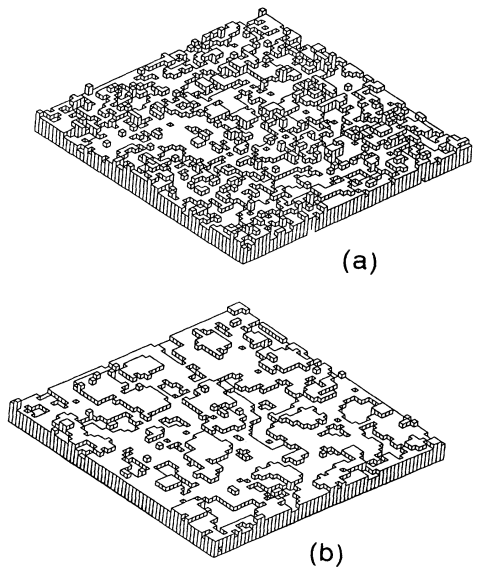

FIG. 5. Effect of surface diffusion on surface morphologies at $\phi/kT=1.6$ and $\Delta\mu/kT=0.69$ without consideration of bulk diffusion. (a) Without surface diffusion; (b) with surface diffusion.

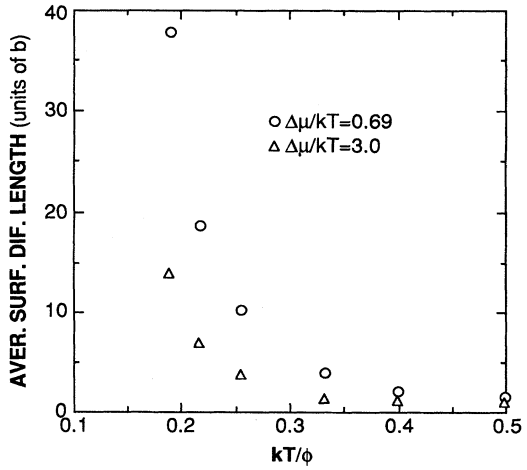

FIG. 6. Dependence of average surface diffusion length on (bond strength)/(temperature) at two different supersaturations, $\Delta\mu/kT=0.69$ and 3.0.

and 5. A mean free path of one lattice unit implies an extremely dense nutrient similar to a liquid. It is evident from this figure that bulk diffusion, particularly in the case of a short mean free path [Fig. 7(c)], destabilizes the surface morphology. With increasing surface roughness, not only is the stabilizing effect of surface diffusion weak, but simultaneously the stabilizing anisotropy in surface kinetics is decreased. Once a protrusion forms by chance, it will be amplified by the bulk diffusion. At intermediate values of temperature and supersaturation, there exists a competition between surface kinetics and bulk diffusion. Only if the surface kinetics prevails can crystal surfaces remain stable, i.e., faceted.[16] More pronounced destabilization from bulk diffusion at higher temperatures will be shown later.

2. *Supersaturation effects*

Increases in supersaturation can also affect the crystal morphology through kinetic roughening.[41–44] This is also born out by our 2D simulations.[15,16] The influence of supersaturation on a 3D growth morphology is shown in Fig. 8, in which the temperature and bond strength are kept constant ($\phi/kT=3.9$). Both surface and bulk diffusion are included. One sees that, with increasing supersaturation, the size of the 2D clusters decreases, and the surface roughens, eventually leading to many depressions and protrusions on the surface and even vacancies in the crystal. As formulated in Sec. II A, an increase in supersaturation causes an increase in impingement rate [Eq. (2)] and hence a relative decrease in evaporation probability [Eq. (6)]. When the supersaturation reaches some critical value, the surface kinetics become relatively less important and the growth process is controlled by bulk diffusion. The ensuing loss of facet stability is further illustrated in Fig. 9 by profiles of the interfacial layer occupation numbers. The four profiles correspond to the cases depicted in Fig. 8. One clearly sees that the interfacial width grows with increasing supersaturation.

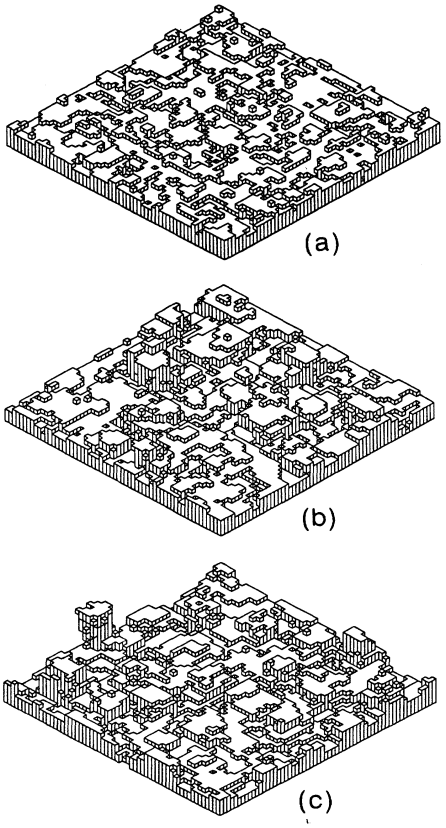

FIG. 7. Effect of the mean-free-path length in bulk diffusion on surface morphologies at $\phi/kT=2.3$ and $\Delta\mu/kT=3.0$. Surface diffusion is included. (a) $|a|=\infty$, (b) $|a|=10b$, (c) $|a|=1b$.

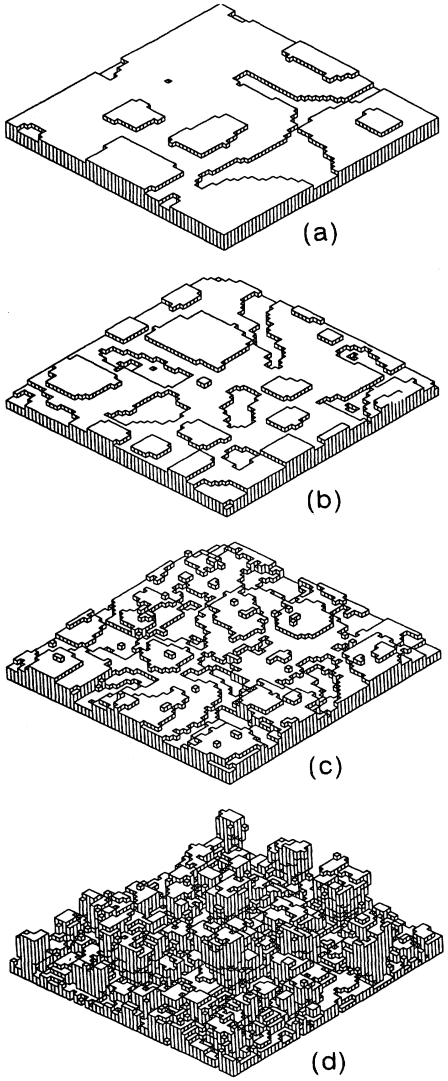

FIG. 8. Effect of supersaturation on surface morphologies at $\phi/kT=3.9$ and a mean free path of one lattice unit. (a) $\Delta\mu/kT=0.69$, (b) $\Delta\mu/kT=3.0$, (c) $\Delta\mu/kT=5.0$, (d) $\Delta\mu/kT=7.0$.

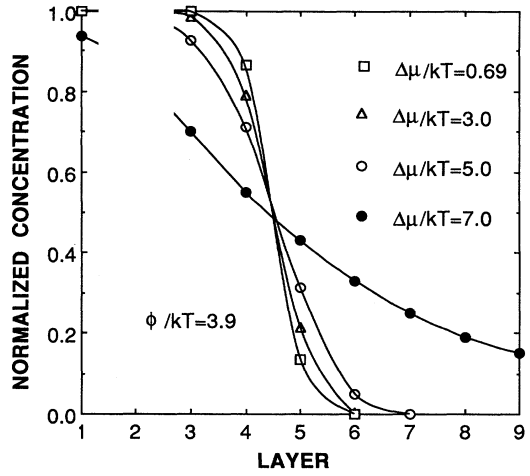

FIG. 9. Coverage of interfacial layers in the surface morphologies of Fig. 8.

The above results reveal significant concentrations of overhangs and vacancies in the crystal at higher supersaturations and temperatures. Hence, under these conditions, the SOS (no overhang) assumption is unrealistic for the description of crystal growth morphologies. Thus the SOS assumption is only a good approximation at low temperatures and supersaturations where the surface morphology is controlled by surface kinetics rather than bulk diffusion. Note, however, that the supersaturation value required for significant kinetic roughening depends on both bond strength and temperature. A crystal surface can have the same roughness at different combinations of supersaturation and temperature.

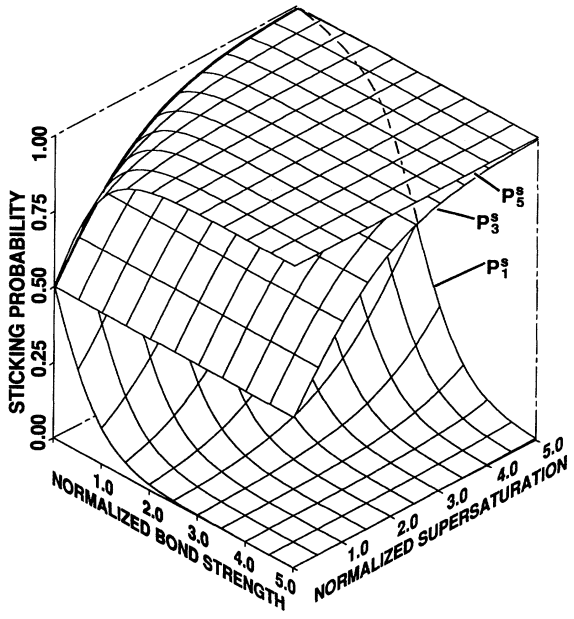

FIG. 10. Sticking probability P_i^s [Eq. (9)] as a function of ϕ/kT and $\Delta\mu/kT$. For clarity, only P_1^s, P_3^s, and P_5^s are shown.

In order to illustrate the dependence of the anisotropy in interface kinetics parameters on growth conditions, we have plotted in Fig. 10 the sticking probabilities at sites with various numbers of nearest neighbors as a function of (temperature)/(bond strength) and supersaturation [Eq. (9)]. For clarity only surfaces for P_1^s, P_3^s (kink site), and P_5^s are plotted in this figure. Note the temperature independence of P_3^s that results from the assumption of local equilibrium at the kink site underlying Eq. (9). Figure 10 well illustrates the strong dependence of the anisotropy in sticking probability (separation between P_1^s and P_5^s) on temperature and supersaturation. At low values of these parameters, P_1^s and P_5^s are nearly constant and close to 0 and 1, respectively. This reflects the difficulty of the attachment of isolated particles and the ease with which holes (i.e., sites with more than three solid nearest neighbors) are filled. One can also see from this figure that the anisotropy in sticking probability can be more effectively reduced by increasing the temperature than by increasing the supersaturation. There is a rapid decrease in the anisotropy of the sticking probability around $\phi/kT=1.0$–2.0 at low supersaturation. The value of the anisotropy in sticking probability is a fundamental quantity for controlling the morphology of a crystal surface. Only when the anisotropy is significant can a crystal retain a stable, faceted form.

3. *Surface roughness*

To further quantify the surface morphology features we use a criterion originally introduced by Burton-Cabrera and Frank (BCF)[28] that defines the surface roughness R_s in terms of the surface energy E (i.e., the number of broken bonds times ϕ) at temperature T and the surface energy E_0 for a perfectly smooth surface at zero temperature, in the form

$$R_s=\frac{E-E_0}{E_0} . \tag{12}$$

This R_s is a merely geometrical measure that depends only on the number of broken lateral bonds per unit area. The variation of R_s with temperature obtained from a simulation of an equilibrium situation ($\Delta\mu/kT=0$) is plotted in Fig. 11. One can see that the surface roughness monotonically increases with temperature with a slope that is highly temperature dependent. There is also a unique inflection point (location of maximum slope), which, as better indicated by the plot of the derivative $dR_s/dT(T)$ in the same figure, lies at $kT/\phi\approx 0.62$. Since R_s is proportional to the surface energy, dR_s/dT should be proportional to the heat capacity or specific heat of the surface. A singularity in heat capacity is characteristic for a phase transition. But in MC simulation, the singularity has been degraded owing to the effect of finite system size.[45,46] Swendsen[9] first used a maximum in heat

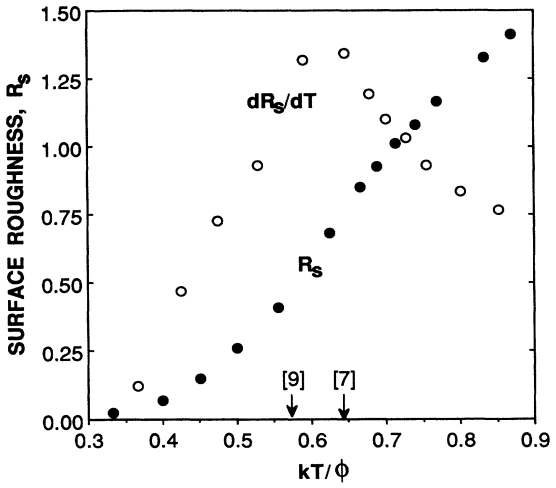

FIG. 11. Surface roughness and its derivative with respect to temperature as function of ϕ/kT at equilibrium ($\Delta\mu/kT=0$). The numbered arrows on the abscissa indicate roughening temperatures obtained earlier by Refs. 7 and 9.

capacity in a MC simulation to define the roughening transition temperature. He obtained for a simple cubic lattice $T_R \approx 0.575\phi/k$. Leamy and Gilmer[7] found, by using a different criterion and employing the SOS restriction, a roughening transition temperature $T_R \approx 0.64\phi/k$, which is surprisingly close to our value. This indicates again that the SOS approximation is appropriate for the description of surface morphology under equilibrium conditions. However, as has been shown above, the SOS assumption is not longer valid when growth becomes bulk diffusion controlled, i.e., the surface has become rough.

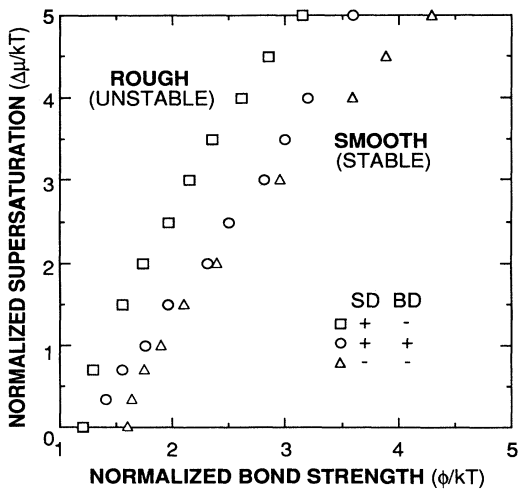

FIG. 12. Stability diagram for smooth (stable) and rough (unstable) growth morphologies as a function of ϕ/kT and $\Delta\mu/kT$. SD: with surface diffusion; BD; with bulk diffusion.

In Fig. 12 we have delineated the temperature-supersaturation combinations for surface roughening transitions as obtained from our MC results and Eq. (12) with the inflection point criterion for systems with various combinations of surface and bulk diffusion conditions. As reflected by the extent of the respective stability regions (smooth versus rough), surfaces on which surface diffusion is significant can retain atomic smoothness up to higher temperatures and/or supersaturations than without surface diffusion. Bulk diffusion, on the other hand, reduces the smooth (stable) region in the ϕ/kT versus $\Delta\mu/kT$ plane, as we have seen more qualitatively before.

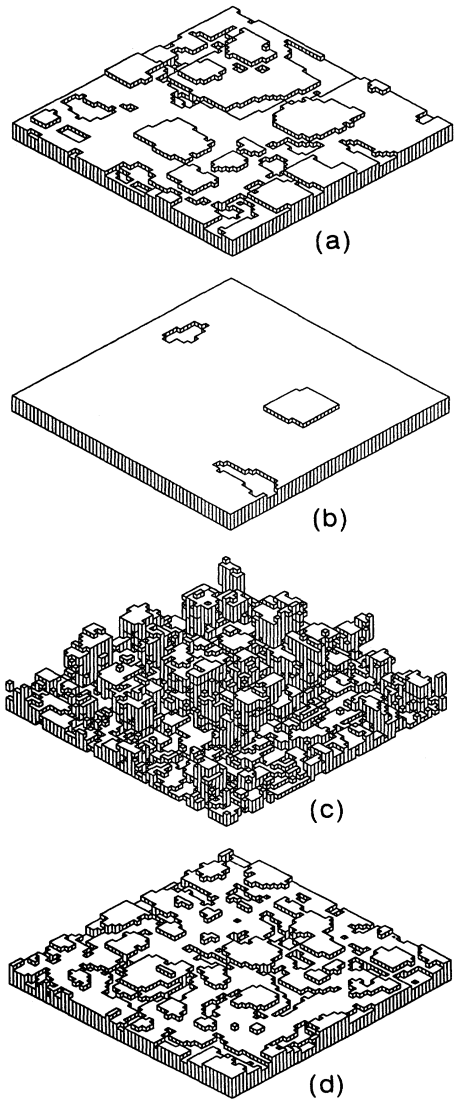

FIG. 13. Effect of noise reduction (multiple registration) (Ref. 15) on surface morphologies at $\phi/kT=3.9$. (a) $\Delta\mu/kT=0.69$, without noise reduction; (b) $\Delta\mu/kT=0.69$, with noise reduction; (c) $\Delta\mu/kT=5.0$, without noise reduction; (d) $\Delta\mu/kT=5.0$, with noise reduction. No reevaporation in all cases.

4. *Reevaporation effects*

All of the above results were obtained with the new algorithm that accounts for the possibility of reevaporation of interfacial particles. To gauge the effect of reevaporation with respect to the earlier noise-reduction algorithm,[15,16] Fig. 13 presents some results obtained without reevaporation and either without or with the multiple-registration scheme used in our earlier work. Otherwise the growth conditions in Figs. 13(a) and 13(b) are the same as in Fig. 8(a) ($\Delta\mu/kT=0.69$) while the conditions in Figs. 13(c) and 13(d) are the same as in Fig. 8(c) ($\Delta\mu/kT=5.0$), with $\phi/kT=3.9$ for all. The multiple-registration noise-reduction scheme[15,16] used for Figs. 13(b) and 13(d) requires ten registrations of incoming particles at a site i before that site is considered occupied. Comparison of the corresponding cases in Figs. 8 and 13 shows that at low supersaturations the noise-reduction scheme is somewhat more effective in smoothing the surface than reevaporation. At high supersaturation, however, both schemes give nearly the same smoothness [compare Figs. 8(c) and 13(d)]. Similar conclusions can be drawn for the smoothing effect of the two schemes upon variations of ϕ/kT. Hence we conclude that at situations far from equilibrium or at high temperatures, the noise-reduction scheme can give qualititatively similar results as the new evaporation scheme, for which, however, the physical implications are much clearer.

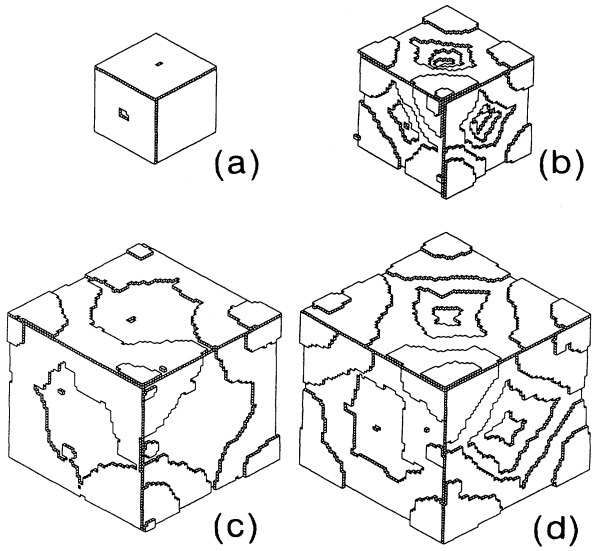

FIG. 14. Growth morphology of three-dimensional cubic crystal in a spherical source at $\phi/kT=2.3$ and $\Delta\mu/kT=0.69$. Noise reduction through multiple registration. (a) and (b), $|a|=1b$; (c) and (d), $|a|=5b$. (a) On addition of 6340 particles to nucleus with $21\times21\times21$; (b) further addition of 31 056 particles to (a); (c) on addition of 28 828 particles to nucleus with $47\times47\times47$; (d) further addition of 52 542 particles to (c).

5. *Spherical source*

The above results were based on the uniform nutrient flux conditions of the planar geometry of Fig. 1(a). But in reality, nutrient flux conditions are most often nonuniform. To further explore the effect of nonuniform supply beyond the 2D results obtained in Refs. 15 and 16 with a circular source, we have performed MC runs with growth onto a cubic surface inside a spherical source; see Fig. 1(b). Figure 14 presents surface morphologies obtained in this geometry with $\phi/kT=2.3$ and $\Delta\mu/kT=0.69$. The mean free path or jump length is one lattice constant, i.e., $|a|=b$ in Figs. 14(a) and 14(b), and five lattice constants ($|a|=5b$) in Figs. 14(c) and 14(d). Similar to the 2D findings in Refs. 15 and 16, one sees that loss of stability of a facet is associated with the formation of depression in its center and, correspondingly, preferred growth at corners and edges. As discussed before,[15,16] this occurs because the anisotropy in surface kinetics can compensate for the nonuniformity in nutrient supply only up to a certain critical size of the crystal. This nonuniformity decreases with increasing mean free path of the diffusing nutrient particles. Hence, as is shown by Fig. 14, the critical crystal size increases with increasing mean free path. To quantify the critical size we have plotted in Fig. 15 the normalized total surface area of the growing cubic crystal versus the size of the crystal. The surface area is normalized by the total surface area (six faces) $6M^{2/3}$ of a perfectly smooth cubic crystal consisting of M growth units. As long as the surface area follows the $6M^{2/3}$ behavior, a crystal is considered morphologically stable. When a crystal begins to lose its stable faceted form, its normalized total surface area increases. Somewhat arbitrarily, we define the critical size as the one at which the surface area exceeds that of a smooth surface by 15%. Thus we find that the crystals depicted in Fig. 14 have critical sizes of about $27b$ and $52b$, respectively,

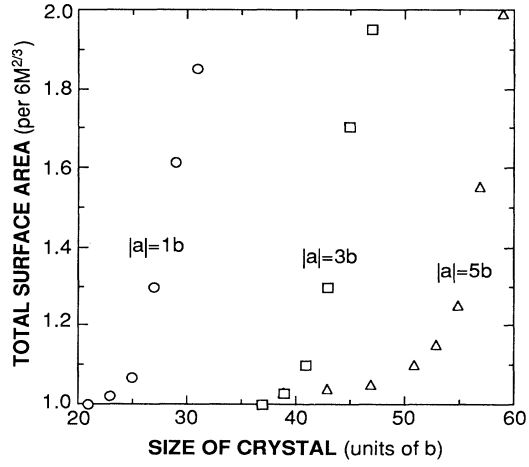

FIG. 15. Normalized total surface area as function of crystal size for a growing cubic crystal. The growth conditions are the same as in Fig. 14.

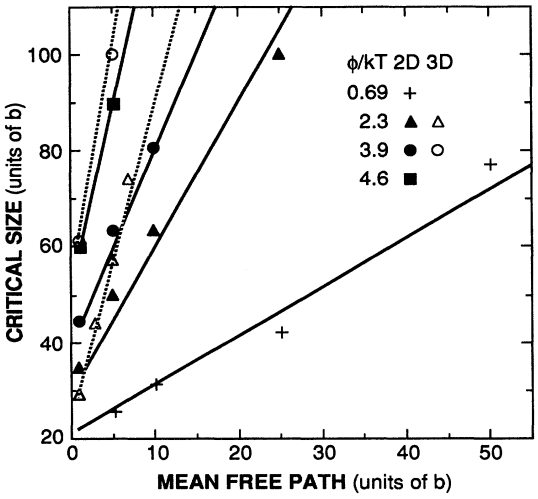

FIG. 16. Dependence of critical size on mean free path at $\Delta\mu/kT=0.69$ and various ϕ/kT for both 2D (Ref. 16) and 3D results.

for $|a|=b$ and $|a|=5b$.

In Fig. 16 we have summarized our 3D results for the dependence of the critical size on mean free path at fixed $\Delta\mu/kT$ and various ϕ/kT's, together with the earlier 2D results.[16] One can see that the critical size increases with decreasing temperature. At fixed temperature and supersaturation, the critical size scales linearly with the mean free path in the parameter range considered. The 3D simulations yield larger slopes than the corresponding 2D cases; i.e., the 3D cases are morphologically more stable. This results from the fact that, on average, there are more solid neighbors associated with interfacial particles in three dimensions and, thus, the (stabilizing) anisotropy in interface kinetics is more pronounced. Although computational time limitations do not allow for the direct simulation of the critical size at the mean free path used in morphological stability experiments,[22–26] Fig. 16 encourages us to scale linearly to these conditions. This leads to an order-of-magnitude agreement between experimental and modeling results for the critical size, with the 3D results approaching the experimental findings closer than the 2D results.[16]

B. Surfaces with dislocations

1. *Temperature effects*

The development of a growth spiral from an initially straight step that results from a screw dislocation with Burgers vector of one lattice constant normal to the (001) face is illustrated in Fig. 17. The (bond strength)/(temperature) (i.e., ϕ/kT) dependence of the surface morphology with a single screw dislocation is shown in Fig. 18. In this simulation, both surface and bulk diffusion were ignored. The supersaturation was kept constant ($\Delta\mu/kT=0.69$) while the ϕ/kT was decreased successively from 5.3, 4.6, 3.0, to 2.0. One sees that at low temperature or high bond strength [Fig. 18(a)] the steps of the resulting growth spiral are quite smooth and the shape is highly polygonized, leaving essentially only low-index steps exposed. As the temperature increased [Figs. 18(b)–18(d)] not only do the steps roughen, but also the shape of the spiral becomes rounder and eventually indiscernible as 2D nucleation becomes pronounced. These morphological changes are a result of the increase in surface roughness with growth temperature. At low temperatures [Fig. 18(a)], growth occurs only via attachment to the spiral steps, since the roughness of the remainder of the facet is too low to result in significant sticking probabilities. Furthermore, due to the low roughness of the steps, the step attachment kinetics is highly anisotropic, leading to rather straight step shapes. As temperature is increased, the steps and remainder of the face roughen. This results in a reduction of the anisotropy in step attachment kinetics and, thus, rounding of the steps. Simultaneously, with increasing face roughness, the energy barrier for 2D nucleation is reduced. On further temperature increase, 2D nucleation-assisted growth becomes increasingly important, until it dominates at $\phi/kT=2.0$.

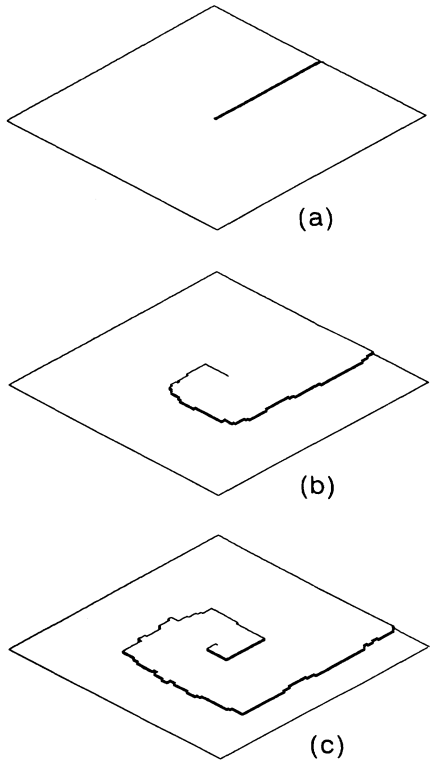

FIG. 17. Time evolution of growth step originating at single dislocation $\phi/kT=5.0$ and $\Delta\mu/kT=0.69$. (a) Initial straight step; (b) after attachment of 1000 particles; (c) after attachment of 5000 particles. Planar source.

These results confirm that it is reasonable to neglect 2D nucleation in simulations of dislocation-assisted growth morphologies at low temperature and supersaturation, where the sticking probability P_1^s (see Fig. 10) is very small. This allows for a drastic reduction in computational times required.[39] Hence, throughout the following simulations of dislocation-assisted growth, the attachment of isolated particles, i.e., with one bond to the surface, is suppressed.

Figure 19 was obtained by considering a pair of screw dislocations with opposite sign, i.e., a Frank-Reed step source.[47] In order to save computer time and memory, the separation between the centers of the dislocations was chosen to be only $7b$. In reality, this separation may be much larger. When the two growth spirals turn in opposite directions and meet, closed loops are formed periodically. During this sequence of simulations the supersaturation was kept constant while ϕ/kT was decreased from 5.3 to 4.6 and 3.9, respectively, and surface and bulk diffusion were ignored. Again, as the temperature increases, the steps become rougher and the closed loops become rounder and spaced more closely, analogous to the temperature-dependent behavior displayed in Fig. 18.

2. *Supersaturation effects*

The effect of supersaturation on the growth morphology of a face with a single screw dislocation is shown in Fig. 20, in which the ϕ/kT is kept at 5.3 while the $\Delta\mu/kT$ is increased successively from 0.69 to 2.0 and 3.0, again ignoring surface and bulk diffusion. As can be seen, increases in supersaturation also make steps rougher and less polygonized, similar to the effect of ϕ/kT in Figs. 18 and 19. This morphological change is, of course, due to kinetic roughening of the steps, in contrast to the thermal roughening occurring as the temperature is increased. In addition, the terrace widths between adjacent spiral arms decrease with increasing supersaturation, consistent with the prediction of classical theories.[28,35–38]

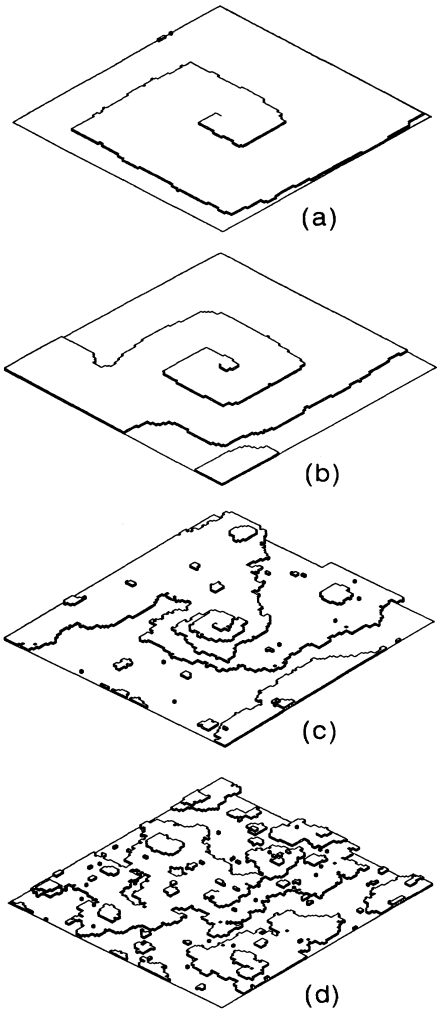

FIG. 18. (Bond strength)/(temperature) dependence of surface morphology of face with a single dislocation. $\Delta\mu/kT=0.69$. Both surface and bulk diffusion are ignored. (a) $\phi/kT=5.3$, (b) $\phi/kT=4.6$, (c) $\phi/kT=3.0$, (d) $\phi/kT=2.0$.

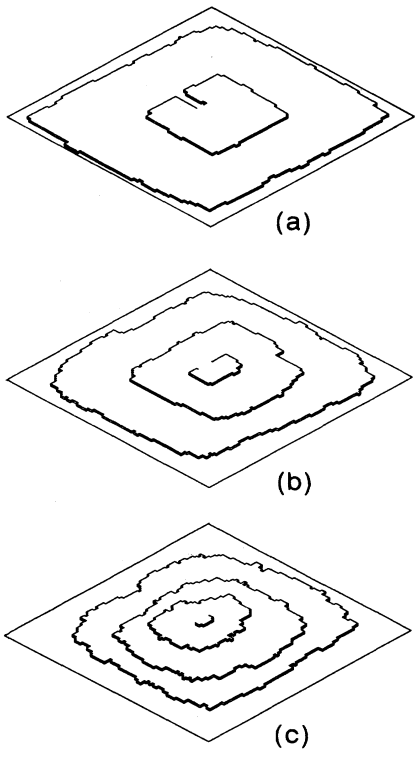

FIG. 19. (Bond strength)/(temperature) dependence of surface morphology of face with a pair of dislocations with opposite sign. $\Delta\mu/kT=0.69$. Attachment of isolated particles suppressed, both surface and bulk diffusion are ignored. (a) $\phi/kT=5.3$, (b) $\phi/kT=4.6$, (c) $\phi/kT=3.9$.

3. *Effects of surface and bulk diffusion*

As has been discussed in Sec. III A, surface diffusion can greatly smooth the morphology of perfect surfaces. The effect of surface diffusion in the presence of a single dislocation is demonstrated in Fig. 21. For this sequence, nutrient bulk diffusion was ignored and the growth conditions (i.e., ϕ/kT and $\Delta\mu/kT$) were the same as those for Fig. 20. We find, in comparison to Fig. 20, not only smoother steps, but also more pronounced polygonization. This is because with surface diffusion, more growth units can reach rounded corners, where, due to the higher kink density, the attachment probability is higher. The spirals also become more polygonized due to the resulting increase in anisotropy of step attachment kinetics. This is at variance with the conclusion of Sunagawa and Bennema,[34] who expected that surface diffusion will suppress the formation of close-packed or periodic-bond-chain oriented steps.

Growth morphologies of a dislocated surface in the presence of both surface and bulk diffusion are depicted in Fig. 22. The growth conditions are the same as in Figs. 20 and 21; i.e., ϕ/kT is kept at 5.3 and the supersaturation is increased. It is evident from this figure that bulk diffusion is also destabilizing for steps, as revealed, for instance, by the lateral depressions at high supersaturation [Fig. 22(c)]. But probably the most interesting new feature revealed by this simulation is the variation of the terrace width, with narrower terraces found near the center of the spiral, particularly at higher supersaturation [Fig. 22(c)]. This is at variance with earlier MC simulations without bulk diffusion[39–41] and classical theories.[8,35–38] Realizing that the above simulation is based on a mean-free-path length (in the bulk) equal to a lattice constant, the decrease in terrace width toward the center of the spiral can be understood as a combined effect of bulk and surface diffusion. Since the growth hillock protrudes into the nutrient, steps and terraces close to its center of the spiral are somewhat better supplied with growth units by bulk diffusion. This leads to tighter winding of the spiral.[28] On the other hand, the surface diffusion fields of terraces at the periphery of the spiral overlap less than those near the center. Overall, this leads to higher spreading velocities of the outer turns of the spiral and, thus, to an increase in terrace width with distance from the spiral's center. In real vapor systems, where $|a| \gg b$, such behavior should not be expected. It is more likely to occur in growth from condensed phases.

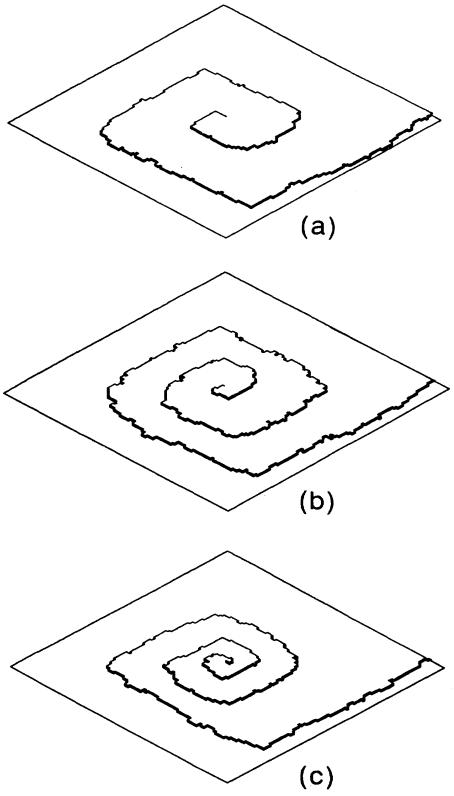

FIG. 20. Supersaturation dependence of surface morphology with a single screw dislocation. $\phi/kT=5.3$. Both surface and bulk diffusion are ignored. (a) $\Delta\mu/kT=0.69$, (b) $\Delta\mu/kT=2.0$, (c) $\Delta\mu/kT=3.0$.

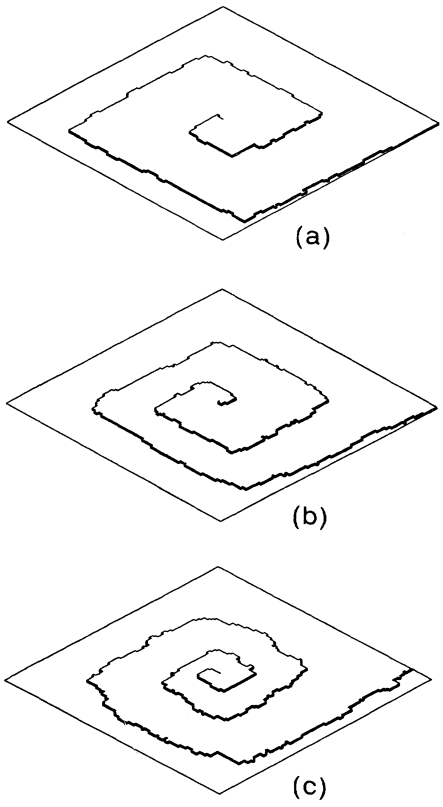

FIG. 21. Effect of surface diffusion on surface morphology with a single screw dislocation. Same growth conditions as in Fig. 20. Bulk diffusion is neglected.

4. *Spherical source*

All of the above results for dislocation-assisted growth were obtained for the planar geometry of Fig. 1(a). To demonstrate the competing effect of 2D nucleation growth and dislocation growth in a nonuniform concentration field, we have carried out a simulation for the 3D geometry of Fig. 1(b) with the same growth conditions as for Fig. 14(a). Among the six faces of the cubic crystal, five are assumed to be perfect and only one has a pair of dislocations with opposite sign. Surface diffusion is taken into account. Figure 23 shows the crystal at a stage after exceeding its critical stable size (see discussion in Sec. III A). The subfigures show different faces of the same crystal, with (a) displaying three of the five faces without dislocation and (b) the dislocated face on top. The dislocation pair is seen to enhance the face stability. All five originally perfect faces have developed central depressions similar to that found in Fig. 23(a). This finding can be understood in terms of the different supersaturation dependence of the growth rate in 2D nucleation and dislocation-assisted growth. Bulk diffusion results in a lower supersaturation in the face center than at the edges and corners. Yet, the face-center region, due to the presence of dislocation-induced surface steps, offers a higher probability for the attachment of growth units than the edge regions in which steps are generated only by 2D nucleation. This increased attachment probability in the center of the face can compensate for the leaner supply of growth units into this region (see also Refs. 15 and 16). This competition of growth steps originating at dislocations in center regions of facets, with growth steps from 2D nucleation near corners, has been experimentally observed by several workers; for references see Ref. 48. Also, the better utilization of growth units (through the anisotropy of kinetics coefficients) in regions that are less readily supplied by the bulk diffusion field is the key point of Chernov's anisotropic stability theory for facet growth.[21]

To further illustrate the competition between 2D nucleation growth and dislocation growth in a nonuniform nutrient field, we have carried out a simulation at a much lower temperature ($\phi/kT=5.3$) than that used for Fig. 23. At the lower temperature, the surface roughness and,

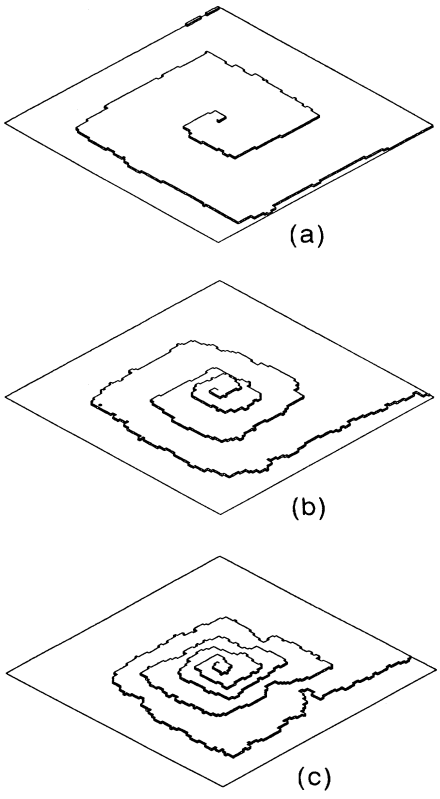

FIG. 22. Effect of surface and bulk diffusion on surface morphology with a single screw dislocation with same growth conditions as in Fig. 20.

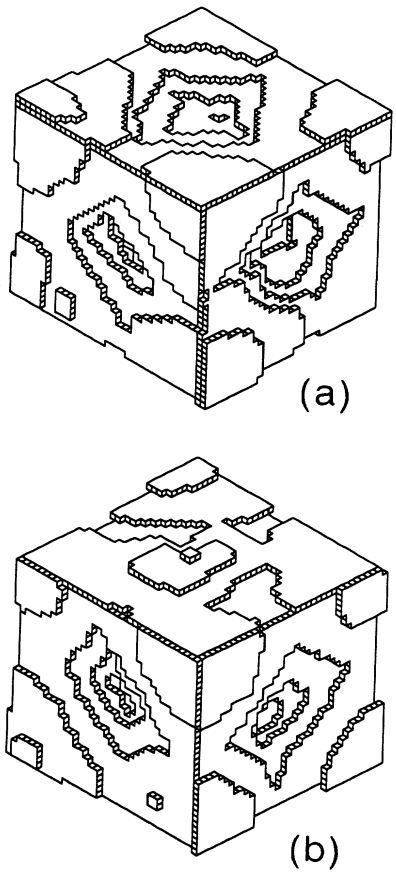

FIG. 23. Growth morphology of a cubic crystal in a spherical source. The growth conditions are the same as in Fig. 14(b). Different faces on the same crystal, (a) all faces without defects, (b) top face with pair of dislocations of opposite sign.

thus, the sticking probability, are considerably reduced. Hence, in order to not exceed prudent computational times, we have modeled only the 3D evolution on one face, with special periodic conditions on the lateral boundaries of the pyramid outlined in Fig. 1(b). Note that the outer boundary condition in this configuration still corresponds to a spherical source as in Fig. 23. In this simulation, ϕ/kT is kept at 5.3, and the supersaturation is increased from 0.6 to 2.0 and 3.0, respectively. The simulations include surface diffusion and unsuppressed attachment of single particles. Figure 24 shows the results after attachment of 20 000 particles in all three cases. One sees that at low supersaturation [Fig. 24(a)] growth occurs only through attachment onto steps that originate at the central dislocation pair. Under these growth conditions, the supersaturation increase at the corners[16] is not high enough to overcome the nucleation barrier for 2D nucleation, which, due to the low surface roughness, is high. The higher supersaturation at the corner, though, destabilizes the dislocation-induced growth step loops, leading to lateral protrusions towards the corners, similar to the growth patterns obtained in the 2D situation.[15,16] Such star-shaped dislocation growth has been observed experimentally; see, for example, Fig. 60 in Ref. 34. As the supersaturation is increased, the controlling effect of the central dislocations decreases and 2D nucleation becomes significant at the corners [Fig. 24(b)]. At an even higher supersaturation [Fig. 24(c)], growth is essentially dominated by 2D nucleation at the corners, in spite of the dislocations at the face center.

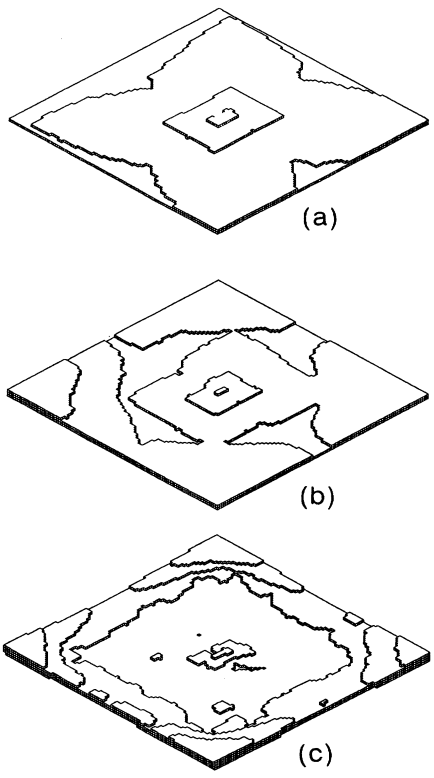

FIG. 24. Growth morphology of a dislocated face in a spherical source at $\phi/kT=5.3$ with bulk and surface diffusion and unsuppressed formation of 2D nuclei. (a) $\Delta\mu/kT=0.69$, (b) $\Delta\mu/kT=2.0$, (c) $\Delta\mu/kT=3.0$.

IV. CLOSING REMARKS

The above simulations, as well as most earlier efforts to model surface morphologies, are based on the (supersaturation)/(temperature) and (bond strength)/(temperature) parameters $\Delta\mu/kT$ and ϕ/kT, respectively. These are highly idealized scaling parameters, which require utmost caution in attempts to *quantitatively* compare the model predictions with actual experiments.

Specifically, it must be reemphasized that, as discussed in Sec. II A in connection with Eq. (2), the chemical-potential difference or supersaturation used in these models is *not equal* to the bulk nutrient supersaturation typically determined by the experimentalist. This chemical-potential difference is solely that part of the overall difference that drives the attachement of growth units once they have been transported to the interfacial region, say to within a mean free path of the growing surface. Though possible in principle, no unambiguous measurements of this interfacial supersaturation have become available as yet. However, all crystal growth theories, as well as measurements of interfacial undercoolings in faceted and nonfaceted regions of an interface that grows from a melt,[49,50] indicate that this interfacial chemical-potential difference necessary to drive a certain attachment (growth) rate depends on the local interface morphology (kink and step density, etc.) and, thus, on the locally governing growth mechanism. This fact is ignored by all modeling at this point by fixing the interfacial $\Delta\mu$ irrespective of the "underlying" surface morphology.

With respect to correlations of the bond or pair interaction energies used in these models with values of actual systems, similar caution is required. In addition to the fact that the simple, highly symmetric bond picture is hardly an accurate representation for actual atomic (quantum-mechanical) interactions, one must realize that the magnitudes for bond strengths are traditionally derived from averaged bulk properties, rather than the (relaxed) surface states that govern the attachment kinetics. Some small improvement of this coarse description, based on a "variable-bond model", has been made by our group earlier.[51]

The above material shows that current kinetic crystal-growth modeling can provide considerable physical insight into the effect of various growth parameters. Yet, it is also clear that much more experimental and theoretical work is required before quantitative fidelity can be expected.

ACKNOWLEDGMENTS

The authors are grateful for the support by the Microgravity Science and Applications Division of the National Aeronautics Administration under Grant No. NAG1-972. This research has also been supported by the State of Alabama through the Center for Microgravity and Materials Research at the University of Alabama in Huntsville, and the Alabama Supercomputer Network.

[1]A. A. Chernov, in *Crystal Growth,* edited by H. S. Peiser (Pergamon, Oxford, 1967), p. 25.
[2]A. A. Chernov and J. Lewis, J. Phys. Chem. Solids **28**, 2185 (1967).
[3]V. O. Esin, V. I. Danilyuk, and V. N. Porozkov, Phys. Status Solidi A **81**, 163 (1984).
[4]V. O. Esin, L. P. Tarabaev, V. N. Porozkov, and I. A. Vdovina, J. Crystal Growth **66**, 459 (1984).
[5]G. H. Gilmer and P. Bennema, J. Crystal Growth **13/14**, 148 (1972).
[6]H. J. Leamy and K. A. Jackson, J. Appl. Phys. **42**, 2121 (1971).
[7]H. J Leamy and G. H. Gilmer, J. Crystal Growth **24/25**, 499 (1974).
[8]H. J. Leamy, G. H. Gilmer, and K. A. Jackson, in *Surface Physics of Materials I,* edited by J. B. Blakely (Academic, New York, 1975), p. 121, and references therein.
[9]R. H. Swendsen, Phys. Rev. B **15**, 5421 (1977).
[10]V. O. Esin and L. P. Tarabaev, Phys. Status Solidi A **90**, 425 (1985).
[11]G. H. Gilmer and P. Bennema, J. Appl. Phys. **43**, 1347 (1972).
[12]H. Müller-Krumbhaar, in *Monte Carlo Methods in Statistical Physics,* edited by K. Binder (Springer, Berlin, 1979), p. 261, and references therein.
[13]P. Bennema and J. P. Van der Eerden, in *Morphology of Crystals,* edited by I. Sunagawa (Terra, Tokyo, 1987), Part A, p. 1; A. A. Chernov and T. Nishinaga, *ibid.*, p. 207.
[14]D. E. Temkin, in *Crystallization Processes* (Consultant Bureau, New York, 1966), p. 15.
[15]R. F. Xiao, J. I. D. Alexander, and F. Rosenberger, Phys. Rev. A **38**, 2447 (1988).
[16]R. F. Xiao, J. I. D. Alexander, and F. Rosenberger, J. Crystal Growth **100**, 313 (1990).
[17]Y. Saito and T. Ueta, Phys. Rev. A **40**, 3408 (1989).
[18]S. Krukowski and F. Rosenberger (unpublished).
[19]W. W. Mullins and R. F. Sekerka, J. Appl. Phys. **35**, 444 (1964).
[20]J. S. Langer, Rev. Mod. Phys. **52**, 1 (1980).
[21]A. A. Chernov, J. Crystal Growth **24/25**, 11 (1974).
[22]C. Nanev and D. Iwanov, J. Crystal Growth **3/4**, 530 (1968).
[23]D. Nenow and V. Stoyanova, J. Crystal Growth **41**, 73 (1977).
[24]C. Nanev and D. Iwanov, Crystal Res. Technol. **17**, 575 (1982).
[25]D. Nenow, V. Stoyanova, and N. Genadiev, J. Crystal Growth **66**, 489 (1984).
[26]M. Staynova and C. Nanev, Crystal Res. Technol. **24**, 951 (1989).
[27]T. A. Witten and L. M. Sander, Phys. Rev. B **27**, 5686 (1983).
[28]W. K. Burton, N. Cabrera, and F. C. Frank, Trans. R. Soc. London Ser. A **243**, 299 (1951).
[29]F. C. Frank, Disc. Faraday Soc. **48**, 67 (1949).
[30]L. J. Griffin, Philos. Mag. **41**, 196 (1950).
[31]H. Bethge, Phys. Status Solidi **2**, 3 (1962).
[32]K. W. Keller, in *Crystal Growth and Characterization,* Proceedings of the ISSCG2 Spring School, Japan, 1974, edited by R. Ueda and J. B. Mullin (North-Holland, Amsterdam, 1975), p. 361.
[33]K. Tsukamoto, J. Crystal Growth **61**, 199 (1983).
[34]I. Sunagawa and P. Bennema, in *Preparation and Properties of Solid State Materials,* edited by W. R. Wilcox (Marcel Dekker, New York, 1982), Vol. 7, p. 1, and references therein.
[35]N. Cabrera and M. M. Levine, Philos. Mag. **1**, 450 (1956).
[36]R. Kaishev, Crystal Growth **3**, 29 (1962).
[37]T. Surek, J. P. Hirth, and G. M. Pound, J. Crystal Growth **18**, 20 (1973).
[38]H. Müller-Krumbhaar, T. W. Burkhardt, and D. M. Kroll, J. Crystal Growth **38**, 13 (1977).
[39]R. H. Swendsen, P. J. Kortman, D. P. Landau, and H. Müller-Krumbhaar, J. Crystal Growth **35**, 73 (1976).
[40]G. H. Gilmer, J. Crystal Growth **35**, 15 (1976).
[41]A. A. Chernov, Ann. Rev. Mater. Sci. **3**, 397 (1973).
[42]C. E. Miller, J. Crystal Growth **42**, 357 (1977).
[43]G. H. Gilmer and K. A. Jackson, in *Current Topics in Materials Sciences,* edited by E. Kaldis and H. J. Scheel (North-Holland, Amsterdam, 1977), Vol. 2, p. 79.
[44]J. D. Weeks, in *Ordering in Strongly Fluctuating Condensed Matter Systems,* edited by T. Riste (Plenum, New York, 1980), p. 293.
[45]K. K. Mon, S. Wansleben, D. P. Landau, and K. Binder, Phys. Rev. Lett. **60**, 708 (1988).
[46]P. Peczak and D. P. Landau, Phys. Rev. B **39**, 11 932 (1989), and references therein.
[47]F. C. Frank and W. T. Reed, Phys. Rev. **79**, 722 (1950).
[48]W. R. Wilcox, J. Crystal Growth **38**, 73 (1977).
[49]J. C. Brice, J. Crystal Growth **6**, 205 (1970).
[50]T. Abe, J. Crystal Growth **24/25**, 463 (1974).
[51]J. -S. Chen, N.-B. Ming, and F. Rosenberger, J. Chem. Phys. **84**, 2365 (1986).